Mata-Díaz, A., López-Puente, J., Varas, D., Pernas-Sánchez, J., & Artero-Guerrero, J. A. (2017). Experimental analysis of high velocity impacts of composite fragments. International Journal of Impact Engineering, 103, 231-240.

doi:https://doi.org/10.1016/j.ijimpeng.2017.01.013

Experimental analysis of high velocity impacts of composite fragments

A. Mata, J. A. Artero-Guerrero, J. Pernas-Sánchez, D. Varas, J. López-Puente

Department of Continuum Mechanics and Structural Analysis. University Carlos III of Madrid. Avda. de la Universidad, 30. 28911 Legans, Madrid, Spain

Abstract

In this work the behaviour of carbon/epoxy fragments acting as impactors is analysed. To this end, rectangular pieces of composite laminates were launched at high velocity against a rigid plate in order to study the main failure mechanisms that appear under such conditions. A wide range of impact velocities (from 70 to 180 m/s) was considered in order to study its influence. Using a tracking software the acceleration of the fragment and hence the force time history induced during the impact is obtained. Finally an analytical model is proposed in order to predict the erosion and the impact force.

Keywords: impact, fragment, composite, high-velocity, carbon/epoxy

1. Introduction

The aeronautic industry is an engineering field in which aircraft architects are looking for new solutions in both the structure and the engines in order to decrease the fuel consumption. The fuel cost is one of the main components of the airlines operating costs, and its reduction is crucial for the transport

industry. In addition it is important to highlight that the air transport accounts the 2 % of all greenhouse gases emitted to the atmosphere and the developing of new technologies will diminish the contamination footprint of this industry (in addition a 60% increment in traffic is expected for the next two decades [1]).

Composite laminates exhibit high specific mechanical properties; nevertheless they have low tolerance to impacts when they occur perpendicularly to the laminate plane. Understanding the behaviour of laminates under the aforementioned conditions has become relevant since the use of those materials (in particular carbon/epoxy, CFRP) in aircraft structures has reach approximately the 50% (in terms of weight).

The objects that could impact a CFRP aeronautic structure at high velocity could be classified between hard bodies (metallic fragments) that present higher strength than the CFRP, and do not deform appreciably during the impact, and soft bodies (ice, bird) that get completely deformed during the impact because of its low properties compared to the CFRP. Between those two groups there is an intermediate case, which is the case of a CFRP fragment impacting a CFRP laminate. Since the mechanical properties of both impactor and impacted structure are the same, this impact phenomenon could not be classified in the aforementioned groups.

Composite laminates are increasingly used in aircraft engines components. For instance the new models of engines uses CFRP fan blades which, in case

of an uncontained failure, could impact the CFRP fuselage. In addition the new developments for the single aisle aircraft size include the use of open rotor engines (which present around 20 % less fuel consume) that have a series of counter rotating CFRP blades which could impact the fuselage in case of failure. In the framework of the CleanSky 2 program (which belongs to the Horizon 2020 program of the European Commission) there is an activity which has the objective of demonstrate the performance of this new engine. One of the main challenges of using this new technology, is the need of protection of the aircraft fuselage against the possible impact of one of those blades since in this new design there is no fan case protection. Those examples show the importance of studying the behaviour of carbon/epoxy laminates acting as impactors.

It was not possible to find any work related to the impact of composite fragments at high velocity; neither against a rigid plate, nor against a deformable structure. The most similar works are those that study the high velocity impacts on composite materials (hard bodies or soft bodies), or even the works which analyse the dynamic crushing of composite tubes, which usually are at low velocity. Beginning with the first ones, the behaviour of CFRP laminates under high velocity impact of metallic fragments has been studied by several authors, starting with the works of Cantwell and Morton [2, 3] which were the first ones that analysed the impact process from an experimental point of view. Later, different authors have presented some articles in which numerical or analytical models for CFRP were validated using experimental tests [4, 5, 6, 7, 9, 10]; in those works the impactor was

always a steel fragment launched at velocities ranging from 60 to 500 m/s approximately. All these works analysed the energy absorbed by the laminate during the impact, and also the shape and type of failure induced in the composite. Regarding the numerical models used, they were based on the Hashin and Rotem model [11] the Chang and Chang model [12], and the Hou et al model [13] among others. The authors of the present work have also published several articles analysing the high velocity impact process on composite laminates [14, 15, 16, 17, 18, 19].

The analysis of composite structures subjected to high velocity impact of soft bodies has received less attention. Kim and Kedward [20, 21, 27] studied from an experimental and numerical point of view the high velocity impact of ice on woven composite plates; they found sensible different failure mechanisms compared to the impact of hard bodies, since the ice has little penetration capacity. The authors of the current work have also studied the behaviour of tape laminates under high velocity impacts of ice spheres of different diameters [23, 24, 25]; one of the main conclusions was that delamination is the main failure mechanism that appear in the laminates. Regarding the bird impact on composite laminates, the number of articles is really reduced; one example is the work of Kermanidis et al. [28] in which a leading edge structure is proposed to increase the resistance of a bird impact. It is important to note that usually the works related to bird impact uses as target quite complex structures, and not simple plates which would help to understand the failure mechanism that occur under this kind of impacts.

The dynamic crushing of composite tubes has received also scarce attention. It is possible to find some static analysis and also studies of tubes reinforced with foams or even aluminium. The most relevant studies that analyse the dynamic compression of pure CFRP tubes from a numerical and experimental point of view are the articles of Mamalis et al. [29, 30]. The main objective of those works was related to the study of the energy absorbed during the crashing process.

Since it was not possible to find any work which studies how composite laminates behave as an impactor, it is possible to say that this is the first article that analyses it. Prior to perform a composite fragment impact against a composite panel, it was considered that it will be more interesting to carry out a simpler test in order to study the failure mechanism that appear in the CFRP fragment during the impact. In addition the measurement of the impact force that a composite fragment at high velocity induces is of great interest for the aircraft architects, in order to appropriately design structures that could withstand such kind of loads. The force induced by a composite fragment impact will depend on the flexibility of the structure where it impacts; as the flexibility increases, the force diminishes. When the fragment impacts a rigid plate, the force induced will be the highest possible, and hence it could be considered the worst-case scenario.

In this work composite fragments were launched against a rigid plate. Impacts were carried out at different impact velocities in order to analyse its

influence. A tracking software was used to monitor the fragment movement, which allow by using successive derivatives, to obtain its velocity and its deceleration and hence the impact force. Finally, a simple analytical model is proposed to explain the failure process.

2. Experimental procedure

In order to understand how the composite laminate behaves when acting as an impactor, high velocity impact experimental tests were performed at the Impact Laboratory of the University Carlos III of Madrid (figure 1). The material selected to perform these tests was a composite laminate made using tape prepregs manufactured by Hexcel Composites (AS4 fibre and 8552 epoxy); the plates were manufactured using standard autoclave process. The thickness of the studied laminate was 4 mm (with 21 plies); the ply sequence used was $(45/-45/90/0/90/-45/45/90/0/90/0)_{s'}$. The size of the impactor was $42 \times 100 \quad mm \times mm$. It is important to mention that the fragments were launched along the 0^0 direction.

To accelerate the composite laminate, a 60 mm calibre pneumatic launcher was used. This experimental device uses compressed air at pressures up to 6 bar, to impel the composite fragment through an 18 m long barrel. A special sabot, made of foam, has been developed to hold the specimen during the acceleration. This sabot has to be strong enough not to fail during the acceleration, but also light in order not to interfere with the fragment trajectory; in fact due to its geometry it gets separated from the fragment

Figure 1: One stage pneumatic launcher.

through aerodynamic forces. Impact velocities varied approximately from 70 to 180 m/s; this range of velocities matches with the velocity at which an open rotor blade would impact the aircraft fuselage. In order to measure the impact velocity, a laser barrier was placed close to the muzzle. The composite impacts against a steel plate, which do not deforms plastically during the test. To visualize the impact process, three high speed cameras (a Photron Ultima APX and two SA-Z) have been used; the first one was configured at 20000 frames per second with a resolution of 384×304 pixels, the other two at 100000 frames per second with a resolution of 1024×184 pixels. The lighting was provided by means of two Arrisun HMI lamps of 1800 W. A sketch of the experimental set-up is shown in figure 2.

After the tests, images obtained from the high speed cameras were used to study the movement of the fragment during the impact. A tracking soft-

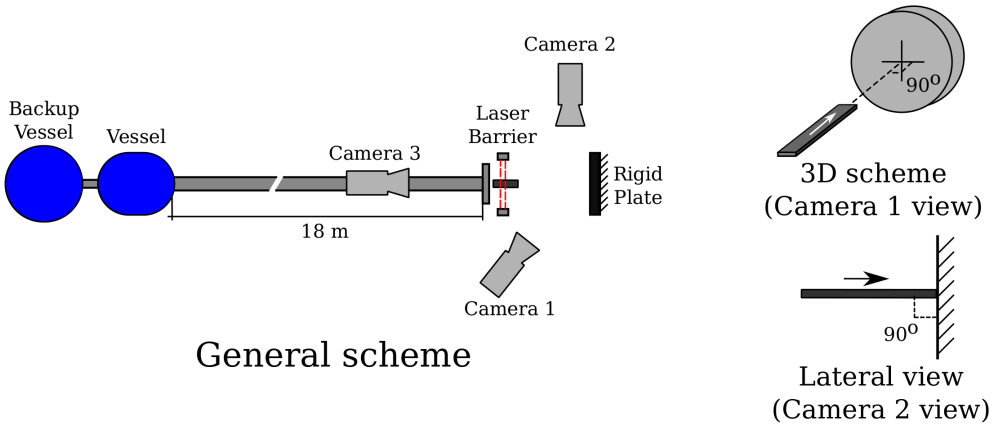

Figure 2: Sketch of the experimental set-up.

ware was used to register the position, and using successive derivatives, the velocity and the acceleration (to estimate the impact force). The composite fragments were marked in order to allow the tracking. The data obtained has some noise due to the fragment vibration caused by the hard contact with the rigid plate; in order to reduce it, a low-pass filter of 15000 Hz has been applied. Figure 3 shows an example of the displacement curve obtained using the tracking software, and the corresponding velocity and acceleration time histories.

3. Experimental results

Experimental tests show that all the impacted specimens have a similar failure pattern. In all of them, a double cantilever beam opening process occurs, accompanied by an important erosion of the middle plies of the laminate. The main failure mechanisms are matrix compressive failure (for the

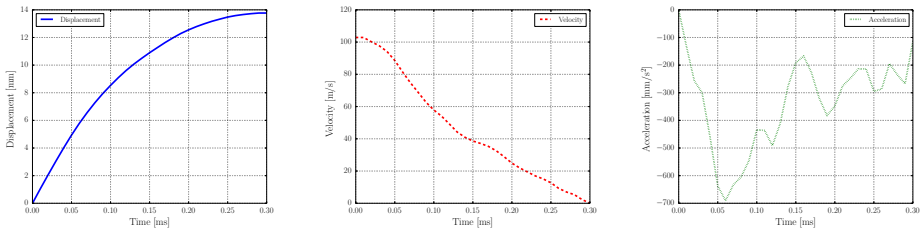

(a) displacement (b) velocity (c) acceleration

Figure 3: Example of the displacement, velocity and acceleration time histories.

90^o and $\pm 45^o$ plies), fibre compressive failure (for the 0^o and $\pm 45^o$ plies), and also delamination (see Figure 4). In addition it is also observed that internal plies present larger erosion than the external.

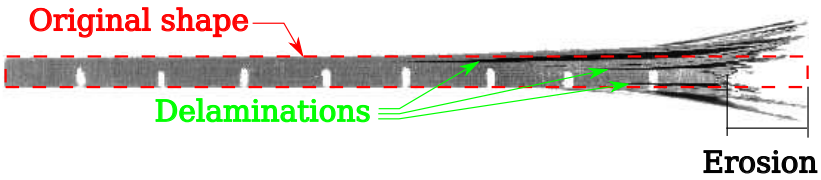

Figure 4: Detailed image of the damaged zone.

The fragment shows the same behaviour during the impact process in the range of velocities considered; in particular four different stages have been identified (Figure 5). The first stage is the contact, in which a compression wave travels from the impact face backwards; as it will be demonstrated later, this wave is strong enough to promote the failure of the laminate (this first step occurs in a very short time period, and hence it could not be observed experimentally). The second stage is the failure, where the laminate front face breaks through compressive failure mechanism, which could include both matrix and fibre failure. The third stage is the opening process, in which the

upper and lower plies of the laminate starts to debond from the middle plies. Finally, in the last stage, the separation of the upper and lower plies and the erosion of the middle zone, promotes a double cantilever beam like failure process. During all the impact process there is no movement of the rigid plate (its movement has also been tracked).

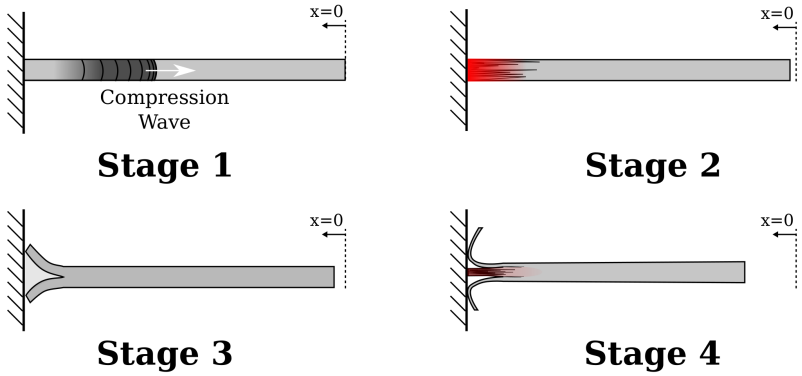

Figure 5: Sketch of the composite fragment impact process.

The images of the impacted specimens (figure 6) suggest a relation between the impacted velocity and the eroded zone, so that as the impact velocity increases, the eroded zone increases.

Figure 7 depicts the eroded distance vs. the impact kinetic energy showing a linear relation between them, which leads to a quadratic relation between the impact velocity and the eroded distance previously observed in the impacted specimens images.

The contact force is obtained experimentally using the variation of linear

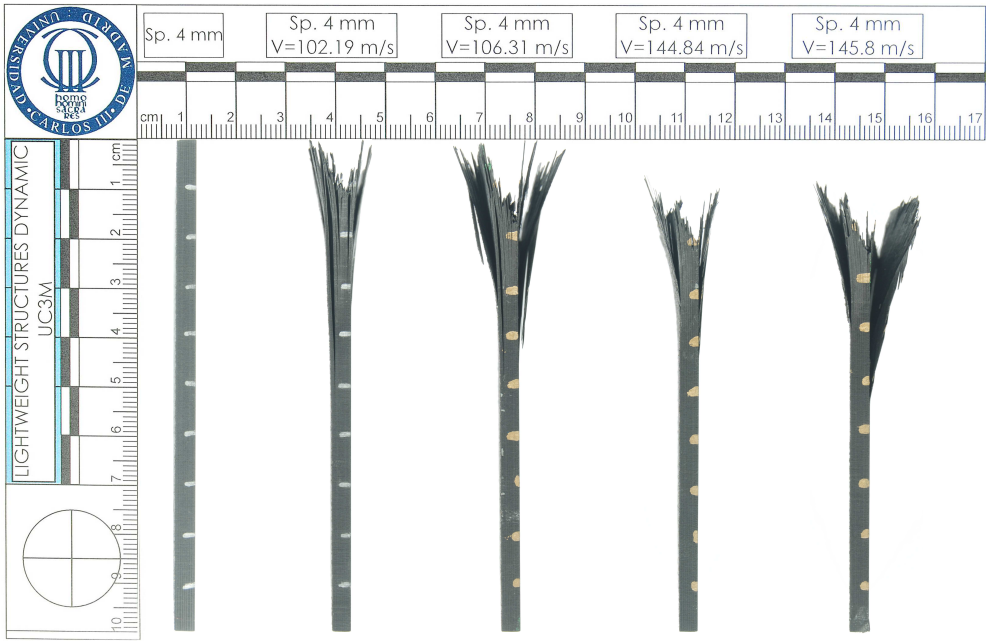

Figure 6: Impacted specimens at increasing impact velocities.

momentum balance:

$$dt\, F = d\,(m\, v) = dm\, v + dv\, m \tag{1}$$

where F is the force acting on the fragment, m is its mass (that varies during the impact), and v its velocity. Assuming a linear decrement of the mass with the fragment position as:

$$m\,(x) = \left(m_i - \frac{m_i - m_f}{x_f} x\,(t)\right) \tag{2}$$

where m_i and m_f are the initial and the final mass respectively, x is the displacement time history, and x_f is the final displacement of the fragment. Then the equation 1 could be written as:

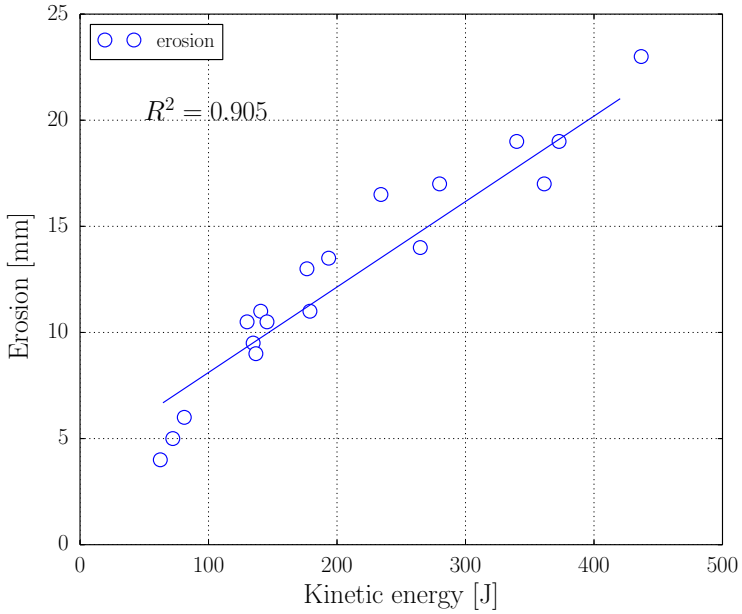

Figure 7: Eroded distance vs. impact kinetic energy, and regression line.

$$F(t) = a(t)\left(m_i - \frac{m_i - m_f}{x_f}x(t)\right) + v^2(t)\ \frac{m_i - m_f}{x_f} \tag{3}$$

where $a(t)$ is the acceleration. Figure 8 shows the impact force time history for different impact velocities, and as it can be seen, all the curves show a similar aspect. All of them present at the beginning an almost linear growing to its maximum value; the higher the impact velocity, the higher the force (as expected). It is important to note that the maximum force occurs at the very beginning of the impact (less than $50\,\mu s$), then the force diminishes reaching the value of zero at approximately $400\,\mu s$. It is possible to differentiate two zones in all the curves: the first one presents a steep slope, which is approximately the same for all impact velocities, and ends in

a maximum that is proportional to the impact velocities. The second one begins in the maximum, and presents a gentle slope in which the curves are cross-linked, and the influence of the impact velocity is much smaller.

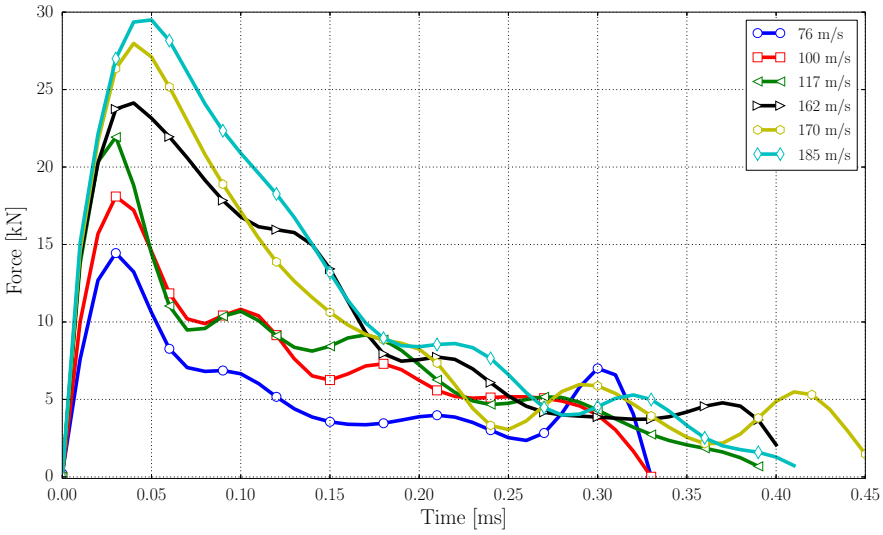

Figure 8: Contact force of the fragment as function of time, for different impact velocities.

Figure 9 shows the impact sequence and the corresponding force time history for an impact performed at 103 m/s. The images are obtained every $30\,\mu s$. The first image corresponds to the instant in which the fragment contact to the rigid plate, being setted to $t = 0\,\mu s$. The maximum force occurs at the very beginning of the impact ($t = 30\,\mu s$), which corresponds approximately with the second image, being the displacement of the fragment 3 mm. Once the failure of the fragment nose is produced, the opening process starts; in the subsequent images (from $t = 60\,\mu s$ onwards) it is possible to observe how this process evolves, and at the same time, how the force decreases.

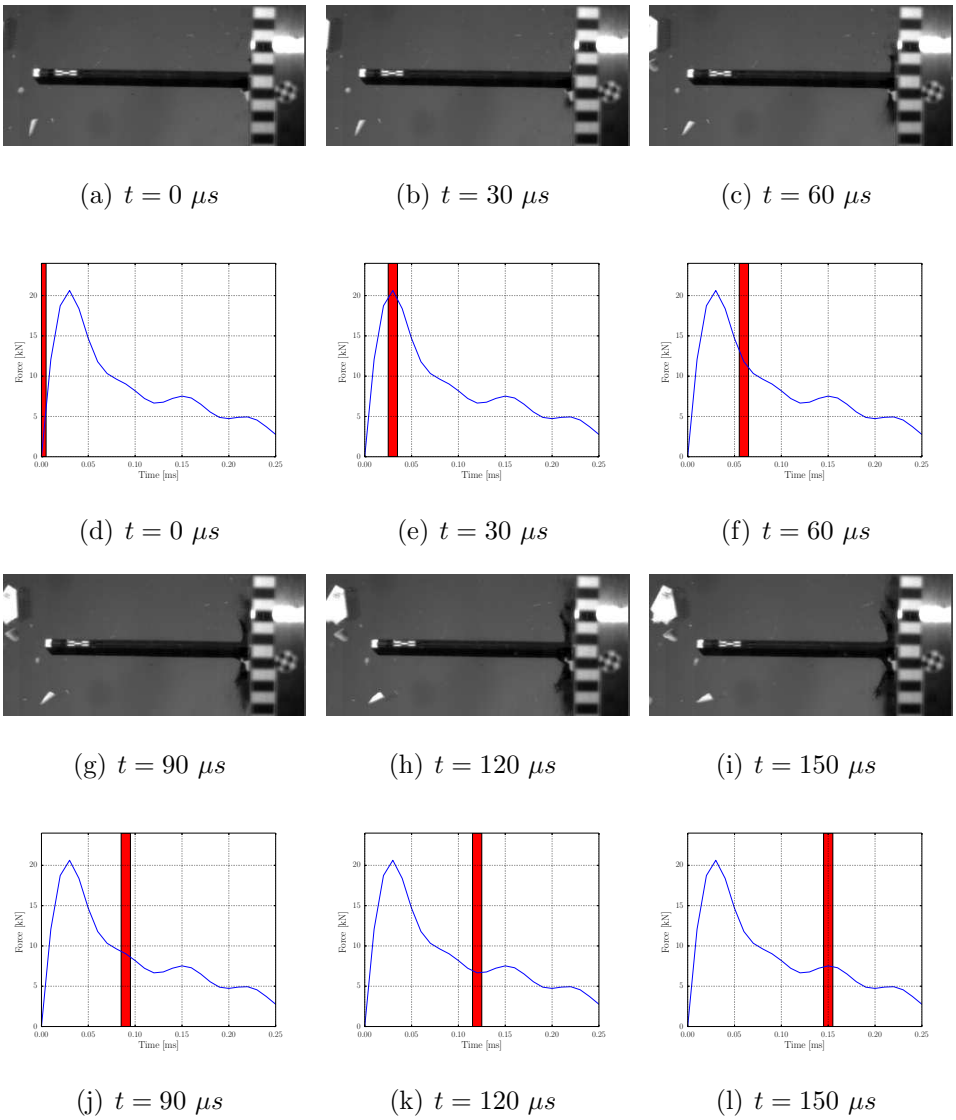

(a) $t = 0\ \mu s$ (b) $t = 30\ \mu s$ (c) $t = 60\ \mu s$

(d) $t = 0\ \mu s$ (e) $t = 30\ \mu s$ (f) $t = 60\ \mu s$

(g) $t = 90\ \mu s$ (h) $t = 120\ \mu s$ (i) $t = 150\ \mu s$

(j) $t = 90\ \mu s$ (k) $t = 120\ \mu s$ (l) $t = 150\ \mu s$

Figure 9: Sequence of the fragment impact at velocity of 103 m/s.

Finally the impulse is calculated for every test, performing the integral of the force time history (figure 10). This figure does not give any new information but it is useful in order to check if the method to calculate the

force is accurate enough (in particular the mass evolution proposed). Since the impulse is also the velocity multiplied by the mass, the slope of the regression line should be the impactor mass (in this case 0.0255 Kg). As it can be seen in figure 10 the impulse of the experimental tests performed, follows a straight line which slope is the impactor mass. This result indicates that the force curves are accurate (since its integral is the mass multiplied by the impact velocity).

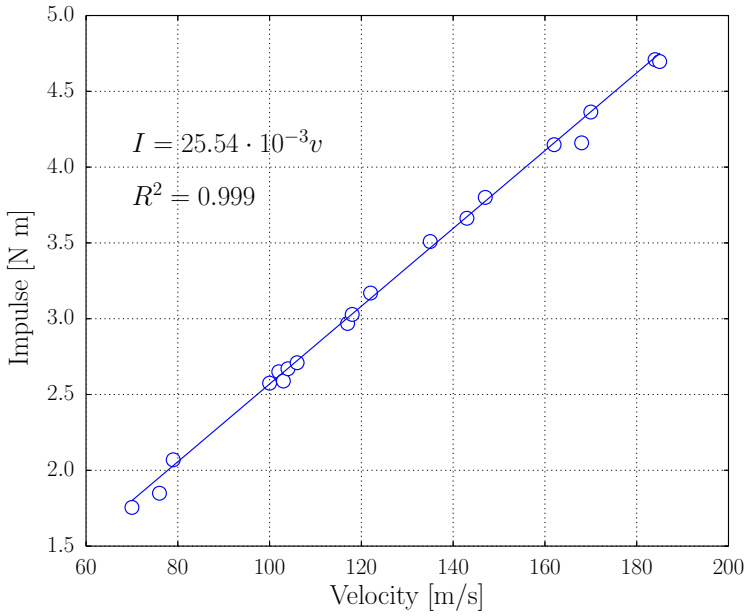

Figure 10: Impulse as function of the impact velocity.

4. Analysis of the impact process

In this section an analysis of the impact process is performed. Impacts against rigid plates could be classified between elastic and non-elastic. The first group considers that no permanent deformation occurs in the object that impacts, and the second one that the object presents permanent deformations after the impact. In order to classify a given impact between the two groups it is possible to use the ratio between the specific energy that the solid could absorb elastically, and the specific kinetic energy: $r_e = \sigma_c^2 / E_{eq}\, v_i^2\, \rho$, where σ_c is the laminate strength under compression, E_{eq} is the equivalent elastic modulus, v_i is the impact velocity, and finally ρ is the fragment density. If this value is greater than the unity, the impact is elastic; in the case studied in this work ($\sigma_c \sim 300\, MPa$, $\rho \sim 1500\, kg/m^3$, $E_{eq} \sim 50\, GPa$), this value is $r_e \sim 0.1$ for an impact of 100 m/s. This value means that the impact is non-elastic (as the impacted specimens suggest).

Another way to analyse the fragment impact is studying the first instants of the contact. If a purely elastic impact is considered, when the fragment contacts the rigid plate, a compressed elastic wave travels at the speed of sound c from the impacted face backwards. When the wave arrives to the rear face of the fragment, it is completely compressed with a deformation that could be estimated as $\varepsilon \sim v_i/c$. During this short period (which is equal to $L/c \sim 20\,\mu s$), the reaction force could be estimated as $F_e \sim \rho\, c\, v_i\, A$, where A is the fragment frontal area. Since the speed of sound of the laminate is approximately $\sim 5 \cdot 10^3\, m/s$, and the impact velocity is $\sim 10^2\, m/s$, the deformation induced is $\sim 2 \cdot 10^{-2}$. It has to be taken into account that the

compress wave is strong enough to promote the failure of the laminate since the failure strain for this laminate is approximately $\varepsilon_f \sim 1 \cdot 10^{-2}$ (using classical laminate theory). In fact the value of the elastic force is $F_e \sim 126kN$ for an impact of $v_i \sim 10^2\ m/s$, which is much higher than the one observed experimentally. This explanation confirms that the impact is non-elastic, since the failure starts just after the impact occurs due to the high deformation induced.

4.1. Analysis of the impact force

The force reaction curves showed in the previous section exhibit a sudden increase in the first instants, reaching a maximum value that is sensible to the impact velocity. Figure 11 shows the maximum force as function of the impact energy; it is possible to observe that as aforementioned, there is an important dependence on the impact velocity. Since the maximum force does not provide all the information of the impact force, figure 11 shows also the its average $\bar{F}$ calculated as:

$$\bar{F} = \frac{1}{t_f} \int_0^{t_f} F\,(t)\, dt \tag{4}$$

where t_f is the total time of the impact. In this case the influence of the impact velocity is similar since it doubles in the range of impact energy analysed. This magnitude its of great importance for designers.

In order to understand the dependence of the impact force with the impact velocity, a linear momentum balance $\Delta t\, F = \Delta\,(m\, v)$ is proposed to estimate

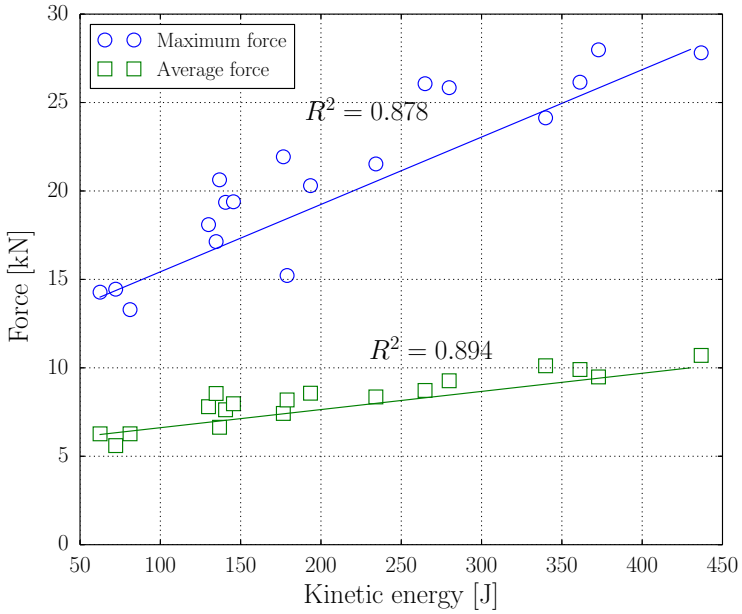

Figure 11: Maximum force and the average of the force as function of the impact energy.

analytically the impact force. This balance is applied to the differential dx (with a mass dm) that gets eroded from the fragment in a period of time dt, in which its velocity variation is v (see figure 12). The balance is:

$$dt\ (F_c - \sigma_c\, A_r) = dm\ v \tag{5}$$

where A_r is the reduced frontal area which is no longer the initial fragment area (is sensibly smaller) because of the large distortion and the opening process, F_c is the contact force, dm is the mass of the differential dx, and v is the current velocity of the fragment. Substituting $dm = dx\, A\, \rho$ (where A is the fragment frontal area), and taking into account that $v = dx/dt$, the balance leads to:

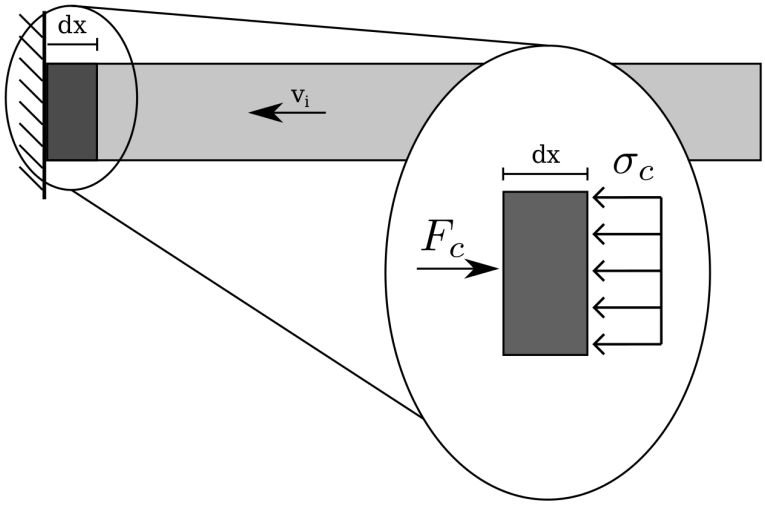

Figure 12: Sketch used to perform the linear momentum balance.

$$F_c = \sigma_c \, A_r + v^2 \, A \, \rho \tag{6}$$

To calculate the contact force it is necessary to take into account some considerations about the first term of the previous expression. The reduced frontal area A_r can be quantified by means of the images obtained in the experimental tests. On figure 13 can be seen that the thickness of the laminate that is eroded is approximately one quarter of the total thickness.

The laminate strength under compression σ_c has strain rate sensitivity, and because of the high velocity impacts studied in this work, it should be taken into account. In order to use an appropriate function to describe the laminate strength under compression, a regression analysis has been performed using the experimental data obtained in different works [**?**]. Figure

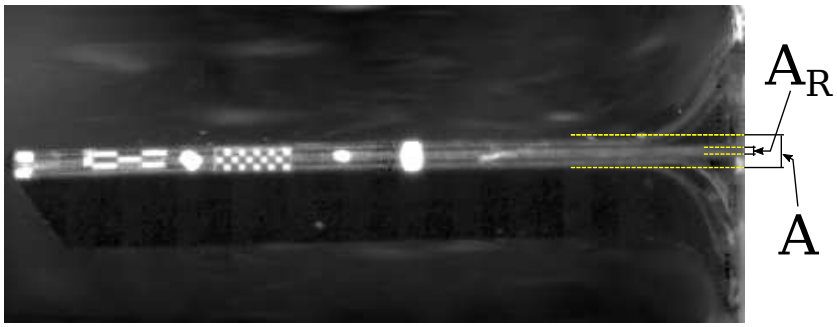

Figure 13: Image of a fragment impacting at 79 m/s.

14 shows the experimental data fitted using a logarithmic function.

Since the strain rate could be written as $\dot{\varepsilon} \sim v/L$, the expression for the contact force could rewritten as:

$$F_c = \left[\sigma_{c0} + c_1 Ln\left(\frac{v}{L\,\dot{\varepsilon}_0}\right)\right] A_r + v^2\, A\, \rho \tag{7}$$

where σ_{c0} and c_1 are the regression constants showed in figure 14, and $\dot{\varepsilon}_0 = 1\ s^{-1}$ (is used only to provide unit consistency). This expression for the contact force (equation 7) has two terms, one is related to the material strength and the other one to the inertia. In the first one there is some dependence on the impact velocity because the laminate strength has strain rate dependence; the second one is clearly dependent on the impact velocity. The ratio of the two terms $r_f = (\sigma_c\, A_r)\,/\,(v^2\, A\, \rho)$ could be used to establish the importance of each one; for an impact velocity of $v = 100\, m/s$ the ratio $r_f \sim 10$ which indicates that in the problem studied in this work, the strength plays a more important role than the inertia.

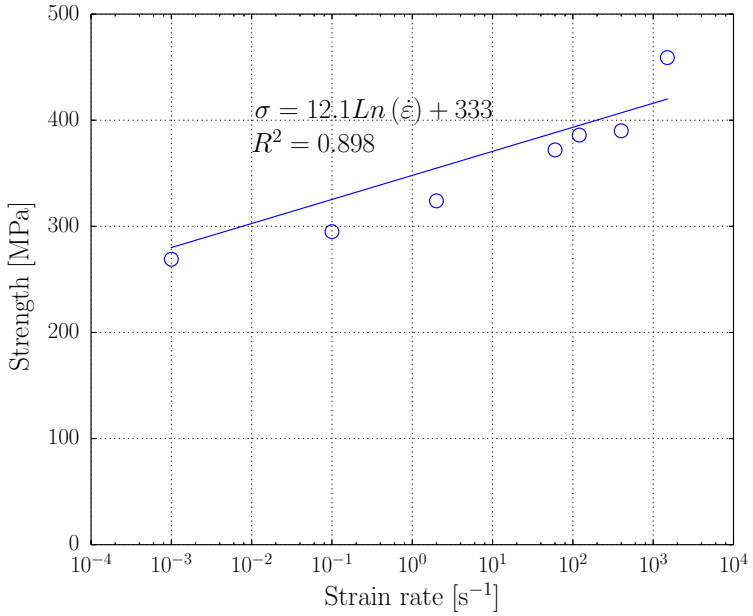

Figure 14: Laminate strength as function of the strain rate.

Finally, in order to check the prediction capacity of the expression obtained for the impact force, equation 7 is plotted against the maximum force obtained experimentally (figure 15). It could be considered that equation 7 gives the maximum impact force when the velocity is sustituted by the impact velocity. As it can be seen in figure 15, the expression predicts adequately the value and the trend of the maximum impact force, with a slight overestimation for low impact velocities. Nevertheless the prediction is good enough taking into account its simplicity.

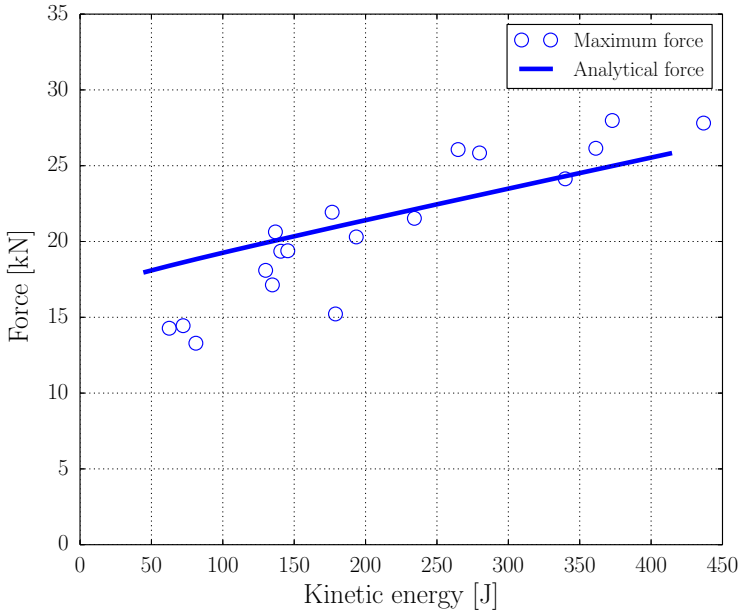

Figure 15: Experimental and analytical maximum impact force as function of the impact energy.

4.2. Analysis of the impact energy

Once the impact force is analysed, an energy balance is proposed in order to determine the relative importance of each of the damage mechanism that appear in the problem. In the impact phenomenon analysed in this work, the initial kinetic energy is absorbed by the laminate (since the final fragment velocity is zero). An analysis of how the different damages absorb the initial kinetic energy of the fragment is performed. To this end an energy balance is proposed; in this balance it is assumed that the lost kinetic energy of the CFRP fragment (which is equal to the initial kinetic energy E_{ki}) is absorbed by three mechanisms, laminate crushing (E_c), delamination (E_d), and the elastic part (E_e):

$$E_{ki} = E_d + E_c + E_e \tag{8}$$

The initial kinetic energy of the projectile is $E_{ki} = (1/2\, m_i\, v_i^2)$. The energy absorbed through laminate crushing could be estimated as $E_c = \sigma_c\, A_r\, y_c$ where y_c is the eroded distance. Regarding the energy absorbed through delamination, the quantity of energy absorbed through this mechanism could be estimated as $E_d = G_{Ic}\, y_d\, w\, n$ where G_{Ic} is the critical energy released in mode I, y_d is the fragment length delaminated, n the number of plies delaminated and w is the fragment width. Finally the absorbed energy in form of elastic deformation could be estimated as $E_e = 1/2\, E_{eq}\, \varepsilon_f^2\, w\, L\, h$, where L is the fragment length, and h the fragment thickness. Equation 8 could be rewritten as:

$$\frac{1}{2}\, m_i\, v_i^2 = \sigma_c\, A_r\, y_c + G_{Ic}\, y_d\, w\, n + \frac{1}{2}\, E_{eq}\, \varepsilon_f^2\, w\, L\, h \tag{9}$$

In order to estimate the importance of each term, the ratio between each of the absorption mechanisms and the kinetic energy lost during the impact is estimated. To quantify it, table 1 shows the approximate values of the parameters that appear in equation 9.

The ratio between the energy absorbed through laminate crushing and the kinetic energy lost by the projectile could be written as:

$$\frac{E_c}{E_{ki}} = \frac{2}{1}\frac{\sigma_c\, A_r\, y_c}{m_i\, v_i^2} \sim 1 \tag{10}$$

variable	value
σ_c	$\sim 10^8\, MPa$
m_i	$\sim 10^{-2}\, kg$
v_i	$\sim 10^2\, m/s$
A_e	$\sim 10^{-4}\, m^2$
y_c	$\sim 10^{-2}\, m$
y_d	$\sim 10^{-2}\, m$
G_{Ic}	$\sim 10^2\, J/m^2$
w	$\sim 10^{-2}\, m$
L	$\sim 10^{-1}\, m$
h	$\sim 10^{-3}\, m$
n	~ 10
E_{eq}	$10^{10}\, MPa$
ε_f	10^{-2}

Table 1: Characteristic values of the variables that appear in the problem.

The ratio between the energy absorbed through delamination and the kinetic energy lost by the projectile could be written as:

$$\frac{E_d}{E_{ki}} = \frac{2}{1}\frac{n\, G_{Ic}\, y_d\, w}{m_i\, v_i^2} \sim 10^{-3} \tag{11}$$

Finally the ratio between the energy absorbed through elastic deformation and the kinetic energy lost by the projectile could be written as:

$$\frac{E_e}{E_{ki}} = \frac{E_{eq}\, \varepsilon_f^2\, h\, w\, L}{m_i\, v_i^2} \sim 10^{-2} \tag{12}$$

The analysis of the previous results allows to conclude that the main absorption mechanism is the laminate crushing, which is two order of magnitude more relevant than the energy absorbed by elastic deformation and three than the energy absorbed through delamination.

5. Analytical model

In the previous section it was identified that the main failure mechanism of the fragment is the laminate crushing. Using this hypothesis an energy balance is proposed in order to determine the fragment erosion. Equalling the kinetic energy lost by the fragment in a dx, to the energy absorbed through crushing, the differential equation in terms of a differential energy balance is:

$$-\frac{1}{2}d\left(m\left(x\right)\ v\left(x\right)^2\right) = \sigma_c\left(\dot{\varepsilon}\right)\ A_r\, dx \tag{13}$$

where x is the fragment displacement, $m\left(x\right)$ and $v\left(x\right)$ are the fragment mass and velocity respectively at a given displacement x, and $\sigma_c\left(\dot{\varepsilon}\right)$ is the laminate strength under compression that is function of the strain rate (previously defined). In equation 13 it is assumed that all the fragment has the same velocity for a given displacement. In the previous section an expression for describing the influence of the strain rate sensitivity on the laminate strength under compression was determined. Substituting the strength function $\sigma_c = \sigma_{c0} + c_1 Ln\left(\dot{\varepsilon}/\dot{\varepsilon}_0\right)$, equation 13 could be written (using $\dot{\varepsilon} \sim v/L$) as:

$$-\frac{1}{2}\frac{d\left(m\left(x\right)\ v\left(x\right)^2\right)}{dx} = \left[\sigma_{c0} + c_1 Ln\left(\frac{v\left(x\right)}{L\,\dot{\varepsilon}_0}\right)\right]\ A_r \tag{14}$$

In this equation the mass evolution is considered to be linear with the fragment displacement $m\left(x\right) = m_i\ \left(L - x\right)/L$ (as previously described). In order to adimensionalize equation 14 the following variable changes are performed: $x^* = x/L$ and $v^* = v/v_i$. The mass evolution could be written as: $m\left(x^*\right) = \left(1 - x^*\right)\ m_i$:

$$-\frac{v_i^2}{2\,L}\frac{d\left(m\left(x^*\right)\ v^*\left(x^*\right)^2\right)}{dx^*} = \left[\sigma_{c0} + c_1 Ln\left(\frac{v_i\,v^*\left(x^*\right)}{L\,\dot{\varepsilon}_0}\right)\right]\ A_r \tag{15}$$

In order to obtain an easy solution, another variable change is proposed $w^* = \left(v^*\right)^2$. In addition the differentiation in the left size is done (from now the asterisk will be omitted for more clarity):

$$-\frac{v_i^2}{2\,L}\left(\frac{dm\left(x\right)}{dx}w\left(x\right) + \frac{dw\left(x\right)}{dx}m\left(x\right)\right) = \left[\sigma_{c0} + c_1 Ln\left(\frac{v_i\,w\left(x\right)^{1/2}}{L\,\dot{\varepsilon}_0}\right)\right]\ A_r \tag{16}$$

Substituting the mass function, and rearranging the terms equation 16 leads to:

$$\frac{dw}{dx} - \frac{w}{1-x} + \frac{L\,A_r c_1}{m_i\,v_i^2}\frac{Ln\,(w)}{1-x} = -\frac{1}{1-x}\frac{2\,L\,A_r}{m_i\,v_i^2}\left[\sigma_{c0} + c_1 Ln\left(\frac{v_i}{L\,\dot{\varepsilon}_0}\right)\right] \quad (17)$$

In order to simplify the previous expression the constants are grouped. The constants that multiply the logarithm of w represents the ratio between the energy absorbed through laminate crushing due to the strength increment because of the strain rate sensitivity, and the initial kinetic energy of the fragment:

$$\alpha = \frac{L\,A_r c_1}{m_i\,v_i^2} \quad (18)$$

This constant is approximately $\alpha \sim 0.2$ for an impact energy of $v_i = 100 m/s$. The other constant that stays on the right hand side of the equation, represents the ratio between the energy absorbed through laminate crushing and the initial kinetic energy of the fragment:

$$\beta = \frac{2\,L\,A_r}{m_i\,v_i^2}\left[\sigma_{c0} + c_1 Ln\left(\frac{v_i}{L\,\dot{\varepsilon}_0}\right)\right] \quad (19)$$

The value of this constant is $\beta \sim 14$ for an impact energy of $v_i = 100\,m/s$. The equation could be rewritten as follows:

$$\frac{dw}{dx} - \frac{w}{1-x} + \alpha\frac{Ln\,(w)}{1-x} = -\frac{\beta}{1-x} \quad (20)$$

To solve this equation, the initial condition $w\,(0) = 1$ should be used. A closed form solution could not be found for this differential equation. Since this equation is adimensionalized, it is possible to state that the order of

magnitude of the first two terms is the unity and, since $\alpha < 1$, the order of magnitude of the third one is 10^{-1}. Hence an expansion in the form of $w = w_{(0)} + \alpha\, w_{(1)}$ is proposed. Assuming this simplification, the order of magnitude of the error will be α^2. The equation for the zero order could written as:

$$\begin{cases} \dfrac{dw_{(0)}}{dx} - \dfrac{w_{(0)}}{1-x} = -\dfrac{\beta}{1-x} \\ w_{(0)}\left(0\right) = 1 \end{cases} \tag{21}$$

which have a simple closed solution, which is:

$$w_{(0)}\left(x\right) = \beta\frac{x}{x-1} + \frac{1}{1-x} \tag{22}$$

The first order differential equation could be written as:

$$\begin{cases} \dfrac{dw_{(1)}}{dx} - \dfrac{w_{(1)}}{1-x} + \dfrac{Ln\left(w_{(0)} + \alpha\, w_{(1)}\right)}{1-x} = 0 \\ w_{(1)}\left(0\right) = 0 \end{cases} \tag{23}$$

Using the Taylor series expansion the logarithm could be approximated to:

$$Ln\left(w_{(0)} + \alpha\, w_{(1)}\right) \sim Ln\left(w_{(0)}\right) + \alpha\frac{w_{(1)}}{w_{(0)}} + O\left(\alpha^2\right) \tag{24}$$

and retaining only the first term, equation 23 leads to:

$$\begin{cases} \dfrac{dw_{(1)}}{dx} - \dfrac{w_{(1)}}{1-x} + \dfrac{Ln\left(w_{(0)}\right)}{1-x} = 0 \\ w_{(1)}\left(0\right) = 0 \end{cases} \tag{25}$$

which haves the following closed form solution:

$$w_{(1)}(x) = -\frac{Ln(1-\beta\,x)}{\beta\;(x-1)} + \frac{x\;Ln\left(\frac{\beta\,x-1}{x-1}\right)}{x-1} + \frac{Ln(1-x)}{x-1} \tag{26}$$

In order to determine the eroded distance, the kinetic energy of the fragment as function of the fragment position is equalled to the kinetic energy lost by the fragment E_{ki}.

$$E_k(x) = \frac{1}{2} m(x) \left[\left(w_{(0)} + \alpha\, w_{(1)}\right) v_i^2\right] \tag{27}$$

It is easy to observe that it is not possible to find a closed solution for x when equalling the complete solution to the kinetic energy lost by the fragment E_{ki}. Nevertheless using the zero order solution it is possible to obtain an approximation for the eroded distance. In this case the kinetic energy as function of the distance x is:

$$E_k(x) = \frac{1}{2} m(x)\; v^2(x) = \frac{m_i\, v_i^2}{2} \left(\frac{L-x}{L}\right) \left(\frac{L-\beta\,x}{L-x}\right) \tag{28}$$

Taking into account that the initial kinetic energy is absorbed into damage, it is possible to obtain the eroded distance x_e, equalling $E_c(x) = 0$ (when the fragment stops), which leads to:

$$x_e = \frac{L}{\beta} = \frac{m_i\, v_i^2}{2\, A_r} \left[\sigma_{c0} + c_1 Ln\left(\frac{v_i}{L\,\dot{\varepsilon}_0}\right)\right]^{-1} \tag{29}$$

In this last expression the eroded distance increases with the impact velocity and with the mass, and diminishes with the contact area and the laminate strength; all this results are expected. Using a similar approach, the eroded mass could be determined using:

$$m_e = \frac{m_i}{\beta} = \frac{m_i^2\, v_i^2}{2\, L\, A_r} \left[\sigma_{c0} + c_1 Ln \left(\frac{v_i}{L\, \dot{\varepsilon}_0} \right) \right]^{-1} \tag{30}$$

The error of this two last approximations is of the same order of α, so around 20% for an impact velocity of $v_i = 100\, m/s$. Figure 16 shows at the left the eroded distance vs. the impact velocity for both experimental data and analytical model, and at the right the eroded mass for both experimental data and analytical model. In both cases the predictions are accurate enough to state that the first order of the analytical model predicts adequately the impact phenomenon.

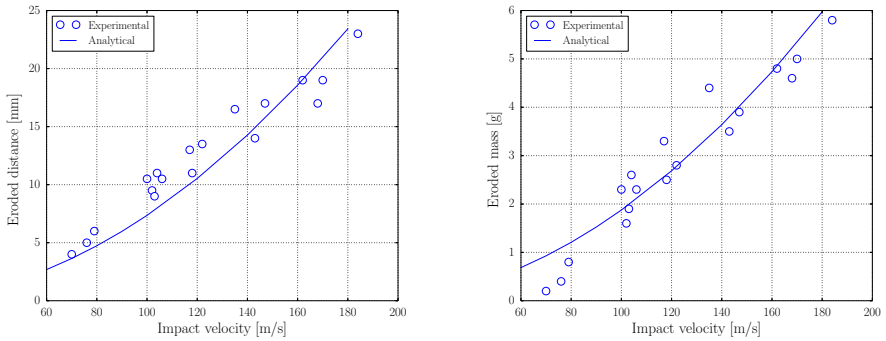

(a) eroded distance (b) eroded mass

Figure 16: Comparison of experimental results and analytical model. Left: eroded distance vs. impact velocity; right: eroded mass vs. impact velocity.

6. Conclusions

In this work the high velocity impact of composite fragments have been analysed. Experimental tests have been performed by means of a gas gun,

and the impact process has been recorded using three high speed video cameras; the images obtained allowed to measure the deceleration of the fragment and hence the force and the impulse induced. An analysis of the failure process has also been performed using the impacted specimens. In addition simplified analytical models have contributed to explain and understand certain aspects of the impact phenomenon. From the results presented and discussed, the main conclusions extracted are:

- The composite fragment, when impacted at high velocity against a rigid plate, fails promoting a double cantilever beam shape. The main failure mechanisms that appear are the matrix and the fibre compressive failure, and also the delamination. Nevertheless it has been proved that the delamination does not contribute substantially in absorbing the kinetic energy of the impact.

- The eroded distance in the composite fragment has found to depend linearly with the kinetic energy of the impact. This is explained by the fact that the erosion of the fragment (matrix and the fibre compressive failure) is the main absorption mechanism.

- The time history impact force shows two different zones; the first one is related to the elastic behaviour of the fragment, and its magnitude varies with the impact velocity. The second one is related with the fragment erosion, and shows little influence on the impact velocity.

- A simple model has been proposed to evaluate the maximum impact force promoted by the fragment. It has been obtained performing a linear momentum balance of an eroded fragment differential.

- A simple model has been proposed to explain how the kinetic energy of the fragment is absorbed. Three mechanisms are distinguished: elastic deformation, delamination and fragment erosion. Analysing the importance of each term it has been concluded that the only mechanism that plays an important role is the last one.

Acknowledgements

This research was done with the financial support of the Spanish Ministry of Economy and Competitiveness under Project reference DPI2013-41094-R.

References

[1] Anderson K,. Bows A. Beyond 'dangerous' climate change: emission scenarios for a new world. Philosophical Transactions of the Royal Society A 2011;369:20-44

[2] Cantwell W, Morton J. Comparison of the low and high velocity impact response of cfrp. Composites 1989;20:545–51.

[3] Cantwell W, Morton J. Impact perforation of carbon fibre reinforced plastic. Compos Sci Technol 1990;38:119–41.

[4] Cantwell W. The influence of target geometry on the high-velocity impact response of cfrp. Compos Struct 1988;10:247–65.

[5] Cantwell W. The influence of fiber stacking-sequence on the high-velocity impact response of cfrp. Journal of Material Science Letters 1988;7:756–8.

[6] Chen J, Allahdadi F, Carney T. High-velocity impact of graphite/epoxy composite laminates. Compos Sci Technol 1997;57:1369–79.

[7] Ulven C, VAidya UK, Hosur MV. Effect of projectile shape during ballistic perforation of VARTM carbon/epoxy composite panels. Compos Struct 2003;61:143–50.

[8] Chan S, Fawaz Z, Behdinan K, Amid R. Ballistic limit prediction using a numerical model with progressive damage capability. Compos Struct 2005;77:466–74.

[9] Chan S, Fawaz Z, Behdinan K, Amid R. Ballistic limit prediction using a numerical model with progressive damage capability. Compos Struct 2005;77:466–74.

[10] Sevkat E. Experimental and numerical approaches for estimating ballistic limit velocities of woven composite beams. Int J Impact Eng 2012;45:16–27.

[11] Hashin Z, Rotem A. A fatigue failure criterion for fiber reinforced materials. J Compos Mater 1973;7:448–64.

[12] Chang F, Chang KA. A progressive damage model for laminated composites containing stress concentrations. J Compos Mater 1987;21:834–55.

[13] Hou JP, Petrinic N, Ruiz C, Hallett SR. Prediction of impact damage in composite plates. Compos Sci Technol 2000;60:273–81.

[14] López-Puente J, Zaera R, Navarro C. The effect of low temperatures on the intermediate and high velocity impact response of cfrps. Composites Part B 2002;33:559–66.

[15] López-Puente J, Zaera R, Navarro C. An analytical model for high velocity impacts on thin cfrps woven laminates. Int J Solids Struct 2007;44:2837–51.

[16] López-Puente J, Zaera R, Navarro C. Experimental and numerical analysis of normal and oblique ballistic impacts on thin carbon/epoxy woven laminates. Composites Part A 2008;39:374–87.

[17] Varas D, Artero-Guerrero JA, Pernas-Sánchez J, López-Puente J. Analysis of high velocity impacts of steel cylinders on thin carbon/epoxy woven laminates. Compos Struct 2013;95:923–29.

[18] Pernas-Sánchez J, Artero-Guerrero J, Zahr J, Varas D, López-Puente J. Numerical analysis of high velocity impacts on unidirectional laminates. Compos Struct 2014;107:629–34.

[19] Pernas-Sánchez J, Artero-Guerrero J, Varas D, López-Puente J. Experimental analysis of normal and oblique high velocity impacts on carbon/epoxy tape laminates. Composites: Part A 2014;60:24–31.

[20] H. Kim, K. T. Kedward, AIAA-99-1366 Experimental and numerical analysis correlation of hail ice impacting composite structures, Composite Structures, 68 (1), 1–11 (1999).

[21] H. Kim, K. T. Kedward, Modeling Hail Ice Impacts and Predicting Impact Damage Initiation in Composite Structures, AIAA Journal 38 (7), 1278–1288 (2000).

[22] H. Kim, D. A. Welch, K. T. Kedward, Experimental investigation of high velocity ice impacts on woven carbon / epoxy composite panels, Composites Part A, 34, 25–41 (2003).

[23] Pernas-Sánchez J, Pedroche DA, Varas D, López-Puente J, Zaera R. Numerical modeling of ice behavior under high velocity impacts. Int J Solids Struct 2012;49:1919–27.

[24] Pernas-Sánchez J, Artero-Guerrero JA, Varas D, López-Puente J. Analysis of Ice Impact Process at High Velocity. Exp Mech 2012;55:1669–79.

[25] Pernas-Sánchez J, Artero-Guerrero JA, Varas D, López-Puente J. Experimental analysis of ice sphere impacts on unidirectional carbon/epoxy laminates. Int J Impact Eng 2016;96:1–10.

[26] H. Kim, D. A. Welch, K. T. Kedward, Experimental investigation of high velocity ice impacts on woven carbon / epoxy composite panels, Composites Part A, 34, 25–41 (2003).

[27] H. Kim, D. A. Welch, K. T. Kedward, Experimental investigation of high velocity ice impacts on woven carbon / epoxy composite panels, Composites Part A, 34, 25–41 (2003).

[28] Kermanidis TH, Labeas G, Sunaric M, Ubels L. Development and Validation of a Novel Bird Strike Resistant Composite Leading Edge Structure, Applied Composite Materials 12, 327–353 (2005).

[29] Mamalis AG, Manolakos DE, Ioannidis MB, Papapostolou DP. On the response of thin-walled CFRP composite tubular components subjected to static and dynamic axial compressive loading: Experimental. Compos Struct 2005;69:407–20.

[30] Mamalis AG, Manolakos DE, Ioannidis MB, Papapostolou DP. The static and dynamic axial collapse of CFRP square tubes: Finite element modelling. Compos Struct 2006;74:213–25.

[31] Camanho P, Davila C. Mixed-mode decohesion finite elements for the simulation of delamination in composite materials. NASA/TM-2002-211737 2002;1-37.

[32] Hashin Z, Rotem A. A fatigue failure criterion for fiber-reinforced materials. Journal of Composite Materials 1973;7:448-464.

[33] Matzenmiller A, Lubliner J, Taylor RL. A constitutive model for anisotropic damage in fiber-composites. Mechanics of Materials 1995;125-152.

[34] Turon A, Camanho PP, Costa J, Davila CG. A damage model for the simulation of delamination in advanced composites under variable-mode loading. Mechanics of Materials 2006;1072-1089.

[35] Benzeggagh ML, Kenane M. Measurement of mixed-mode delamination fracture toughness of unidirectional glass/epoxy composites with mixed-mode bending apparatus. Composites Science and Technology 1996;439-449.